HHS Public Access

Author manuscript

Mucosal Immunol. Author manuscript; available in PMC 2024 April 03.

Published in final edited form as:

Mucosal Immunol. 2024 February ; 17(1): 41–53. doi:10.1016/j.mucimm.2023.10.002.

The menstrual cycle regulates migratory CD4 T-cell surveillance in the female reproductive tract via CCR5 signaling

M. Elliott Williams[1], **Felica P. Hardnett**[2], **Anandi N. Sheth**[3], **Alexander N. Wein**[1], **Zheng-Rong Tiger Li**[1], **Jessica Radzio-Basu**[2], **Chuong Dinh**[2], **Lisa B. Haddad**[4], **Elizabeth M.B. Collins**[4], **Igho Ofotokun**[3], **Rustom Antia**[5], **Christopher D. Scharer**[1], **J. Gerardo Garcia-Lerma**[2], **Jacob E. Kohlmeier**[1], **Alison Swaims-Kohlmeier**[1,2,4,✉]

[1]Department of Microbiology & Immunology, Emory University School of Medicine, Atlanta, GA, USA.

[2]Division of HIV Prevention, Centers for Disease Control and Prevention, Atlanta, GA, USA.

[3]Department of Medicine, Division of Infectious Diseases, Emory University School of Medicine and Grady Health System, Atlanta, GA, USA.

[4]Department of Gynecology & Obstetrics, Emory University School of Medicine, Atlanta, GA, USA.

[5]Department of Biology, Emory University, Atlanta, GA, USA.

Abstract

Despite their importance for immunity against sexually transmitted infections, the composition of female reproductive tract (FRT) memory T-cell populations in response to changes within the local tissue environment under the regulation of the menstrual cycle remains poorly defined. Here, we show that in humans and pig-tailed macaques, the cycle determines distinct clusters of differentiation 4 T-cell surveillance behaviors by subsets corresponding to migratory memory (T_{MM}) and resident memory T cells. T_{MM} displays tissue-itinerant trafficking characteristics, restricted distribution within the FRT microenvironment, and distinct effector responses to infection. Gene pathway analysis by RNA sequencing identified T_{MM}-specific enrichment of genes involved in hormonal regulation and inflammatory responses. FRT T-cell subset fluctuations

✉ askohlm@emory.edu .

AUTHOR CONTRIBUTIONS

MEW performed bioinformatic analysis. ANW performed microscopy. ANS and LBH provided clinical tissue specimens. EMBC provided insights and interpretations into the hysterectomy procedure. JR-B assisted with NHP experimentation. FBH and ZTL performed statistical analysis and mathematical modeling. CD performed MVC drug measurements. CDS supervised genomic studies. IO supervised clinical studies. RA supervised mathematical modeling. GG-L supervised and designed the NHP studies. JEK designed experiments, and analyzed data. AS-K supervised, designed, and performed experiments, analyzed data and wrote the paper with assistance from all authors.

DECLARATION OF COMPETING INTEREST

The findings and conclusions of this manuscript are those of the authors and do not necessarily represent the official views of the Centers for Disease Control and Prevention.

The findings and conclusions in this report are those of the authors and do not necessarily represent the official views of the Department of Health and Human Services or the National Institutes of Health.

APPENDIX A. SUPPLEMENTARY MATERIAL

Supplementary data to this article can be found online at https://doi.org/10.1016/j.mucimm.2023.10.002.

were discovered that synchronized to cycle-driven CCR5 signaling. Notably, oral administration of a CCR5 antagonist drug blocked T_{MM} trafficking. Taken together, this study provides novel insights into the dynamic nature of FRT memory CD4 T cells and identifies the menstrual cycle as a key regulator of immune surveillance at the site of STI pathogen exposure.

INTRODUCTION

Genitourinary pathogens, including those that cause sexually transmitted infections (STIs), can lead to a range of severe health complications in women, including pelvic inflammatory disease, cervical cancer, congenital transmission, and stillbirths, highlighting the need for defining correlates of immune protection in the female reproductive tract (FRT). Increasingly, studies report that tissue-resident memory T cells (T_{RM}) are critical for the rapid elimination of many genitourinary pathogens[1–4]. Notably, FRT CD4 T_{RM} has been shown to be necessary for generating immunity against common STIs, including *Chlamydia trachomatis* (*C. trachomatis*) and herpes simplex virus type 2[2,5]. However, it is also important to recognize that CD4 T-cell localization in the FRT may increase susceptibility to human immunodeficiency virus (HIV) infection[6]. These discordant roles for FRT CD4 T cells in disease outcomes underscore the importance of identifying what mechanisms dictate memory CD4 T-cell localization and function within the FRT microenvironment.

Similar to other mucosal tissues, CD4 T-cell migration into the FRT is regulated by specific chemokine receptors and integrins. In response to infection, CCR5, CXCR3, and α4β1 signaling have all been identified as necessary for antigen-specific effector T-cell trafficking from the circulation into both the upper and lower FRT[7,8]. Whereas, in the absence of infection (homeostatic conditions), it is thought that very little T-cell trafficking occurs in or out of the FRT; thus, local recall responses would depend upon tissue-anchored T_{RM}[9,10]. However, distinct from other mucosal tissues, the FRT undergoes extensive and repeated tissue remodeling due to menstruation, and the impact of these processes on cellular immune memory remains poorly defined.

The menstrual cycle, and in particular, the levels and fluctuations of the sex hormones progesterone (P4) and estradiol (E2) are associated with increased infection risk by STI pathogens, including *C. trachomatis, Neisseria gonorrhoeae* (*N. gonorrhoeae*), and HIV[11–13]; although, the immune mechanisms underlying this relationship are unclear. Moreover, while it is known that the cycle drives immune changes throughout the FRT, our understanding of how such alterations affect pre-existing memory T cells and immune protection against pathogen encounter is limited by the scarcity of model systems that experience menstruation[14]. Although menstruation is facilitated by innate immune cells, regulatory and memory T cells have also been reported to exhibit variations over the cycle[13,15]; this suggests that the menstrual cycle might influence local T-cell surveillance against invading pathogens. As the vast majority of women and adolescent girls of reproductive age experience menstruation[16], it is imperative to identify whether and how cycling impacts immune memory in the FRT.

In this study, we used tissue measurements from women along with the pig-tailed macaque (*Macaca nemestrina*) model of the human menstrual cycle to investigate tissue-localized

FRT memory T cells. We found that while T_{RM} did not exhibit overt trends over the menstrual cycle, the vaginal T-cell pool becomes dominated by infiltrating migratory memory T cells (T_{MM}) within the luteal phase. Cytokine analysis and transcriptional profiling identify T_{MM} as a distinct population from both FRT T_{RM} and lymph node memory T cells. Longitudinal profiling over consecutive cycles uncovered periodic waves of T_{MM} immigration corresponding to local CCR5 chemokine production. Finally, we demonstrate that oral administration of a CCR5 antagonist drug inhibited T_{MM} migration, specifically during the luteal phase of the menstrual cycle, while T_{RM} numbers were not significantly altered. Taken together, these results identify that the menstrual cycle dictates a dynamic organization of memory T-cell populations through regulation of CCR5 signaling.

RESULTS

Distinct memory CD4 T-cell populations from cervicovaginal lavage in women are identified by migratory properties

To investigate FRT T-cell surveillance, we first used cervicovaginal lavage (CVL) and blood samples collected from women participants of reproductive age who were exhibiting normal menstrual cycles. T cells enriched from human CVL were then measured for the expression of chemokine receptors and integrins involved in peripheral tissue trafficking (Fig. 1A and B). As compared with matched peripheral blood mononuclear cells (PBMC), CVL CD4 T cells expressed greater CCR5, CCR6, α4β7, and CCR4, which was consistent with previous reports using various FRT sampling methods[17–20]. As expected for T cells residing in nonlymphoid tissue, lymphoid and endothelial adhesion proteins L-selectin (CD62L) and P-selectin levels were reduced. Additionally, the fractalkine receptor, CX3CR1, which functions in T-cell inflammatory trafficking[21], was increased.

Our previous immune characterizations from human CVL identified CCR7 expressing memory CD4 T cells, which are consistent with tissue migratory memory T cells[17,22]. Thus, we asked whether distinct tissue trafficking characteristics could be identified by distinguishing the CVL CD4 T cells. Using participant-matched central memory (T_{CM}: CCR7hi CD45RAlo) or effector memory (T_{EM}: CCR7lo CD45RAlo) CD4 T cells from PBMC to set gating parameters, CVL CD4 T cells were first discriminated for CCR7 expression, followed by measurement of tissue residence (CD69 and CD103) or egress (CD62L) characteristics (Fig. 1C). This analysis showed that CCR7hi CD4 T cells were more likely to also express CD62L but less likely to express CD69 and CD103. Furthermore, Boolean analysis (Fig. 1D) of CD62L, CD69, and CD103 co-expression by CCR7 gating of CVL CD4 T cells identified a profile consistent with peripheral memory T cells that undergo migratory surveillance and recirculation, which we will refer to as T_{MM} ($CD62L^{-}$, $CD69^{+/-}$, $CD103^{-}$)[22–25], while the CVL CCR7lo CD4 T-cell populations predominantly expressed classic tissue retention characteristics ($CD62L^{-}$, $CD69^{+}$, $CD103^{+/-}$; CVL T_{EM} are herein referred to as T_{RM}) consistent with our previous observations[17,26] (Fig. 1D). In addition, comparisons of tissue trafficking properties between the subsets showed that T_{MM} expressed greater CCR6, CX3CR1, CXCR3, CCR4, and P-selectin as compared with T_{RM} (Fig. 1E). No differences in CCR9 or α4β7 were found (not shown). Upon comparing CVL subsets with PBMC T_{CM} and T_{EM}, we found that T_{MM}

trafficking properties were more likely to be significantly different, while T_{RM} expressed greater CCR5 and less P-selectin. Notably, both T_{MM} and T_{RM} expressed greater CCR5 compared with PBMC T_{CM} and T_{EM}, with no difference detected between subsets, and both subsets expressed less CXCR3. These results identified that among the FRT CD4 T-cell pool sampled, CCR7 expression was sufficient to distinguish T cells that were enriched for tissue-itinerant trafficking characteristics, however, both T_{MM} and T_{RM} subsets shared increased CCR5.

Distinctions in the effector responses by vaginal CD4 T-cell subsets are identified in humans and rhesus macaques

Memory T cells residing within mucosal barriers provide rapid and protective effector responses against infection that are critical in immune defense[27,28], but whether FRT T_{MM} and T_{RM} subsets possess distinct effector functions is unknown. Therefore, we first assessed intracellular cytokine production from human CVL CD4 T-cell subsets following a non-specific stimulus (Fig. 1F), which showed that both subsets produced hallmark Th1 cytokines interferon (IFN)γ and interleukin (IL)-2 with little to no IL-17 or IL-10. However, $T_{MM,}$ in contrast to $T_{RM,}$ produced greater IL-2 with less IFNγ. Notably, both populations predominantly produced the pro-inflammatory cytokine tumor necrosis factor (TNF)α, with little to no IL-10 detected, indicating that these cells were not consistent with regulatory T cells. Next, to investigate FRT CD4 T-cell subset responses to antigen-specific stimulation, we measured cytokine production against simian HIV ($SHIV_{162P3}$) using nonhuman primate (NHP) (rhesus macaque) tissues (Supplementary Fig. 1A). CD4 T cells enriched from CVL at 3-weekly intervals of sample collection (post-peak viremia) and from vaginal lamina propria were stimulated with overlapping $SHIV_{162P3}$ envelope peptides *ex vivo* (Supplementary Fig. 1B). As with human samples, we identified T_{MM} in CVL but now also within the vaginal tissues (Supplementary Fig. 1C). Furthermore, IL-2-producing CD4 T cells were detected from both CVL, and vaginal tissue compared with little to no IL-2 responses detected from PBMC CD4 T cells (Supplementary Fig. 1D and 1E). Similar CD4 T cell IFNγ and TNFα production from CVL and vaginal tissue were detected (Supplementary Fig. 1E).

Memory CD4 T-cell characterizations throughout the FRT using intravital labeling in pig-tailed macaques identify compartmental restriction of T_{MM}

Anatomical regions of the FRT (vagina, endocervix, and uterus) comprise distinct mucosal barriers based in part on epithelial composition, mucus production, and tissue-derived signaling interactions[15]. This suggests that FRT T cells might differ in composition or functional characteristics based on localization. Therefore, to define T-cell distribution throughout the FRT environment, we used the pig-tailed macaque model of human menstruation (Fig. 2A)[29]. To first determine CD4 T-cell positioning, we performed immunofluorescence microscopy from vaginal and cervical tissue sections. From vaginal tissues, we identified T cells (TCRαβ expressing cells) at the basal layer of the epithelium, frequently orienting in loose aggregates (Fig. 2B). CCR7 + T cells were also identified in proximity to the basal layer of the vaginal epithelium and progressing towards the apical surface (Fig. 2C). CCR7 + T cells were not detected within cervical tissues (not shown), suggesting preferential localization in vaginal tissues.

To further characterize FRT T cells (including the uterus) in a manner that would enable discrimination of true tissue-localized cells from cells in circulation, we performed intravascular (IV) labeling prior to tissue collection (Fig. 2D and 2E). From the vaginal tissues, T cells were the predominant population among the total leukocyte pool (CD45+ cells) and in contrast to the cervical and uterine regions (Fig. 2F). All FRT tissues exhibited lower mean frequencies of CD4 T cells with higher CD8 T cells in comparison to T cells from draining lymph nodes (dLN), although T-cell ratio comparison by FRT tissue site only showed differences with the cervix (Fig. 2G). Next, we determined CD4 T-cell subset distribution by CCR7 expression (Fig. 2H) and observed that T_{MM} were specifically enriched within the vaginal tissues (Fig. 2I). Notably, while CCR7 expression was mainly restricted to CD4 T cells within the vagina, CD8 T cells throughout the FRT expressed little to no CCR7, consistent with T_{RM}[30]. Then, to determine whether the transcriptional programs of FRT memory CD4 T-cell subsets differed by anatomic localization, we performed bulk RNA sequencing from sorted IV-negative memory (CD45RAlo) CD4 T cells based upon CCR7 expression (Fig. 2J). Because an insufficient number of IV-negative CCR7 expressing CD4 T cells were recovered from the cervical and uterine tissues, only T_{MM} from the vaginal tissues was used for this analysis. Principal component analysis (PCA) showed that memory CD4 T-cell populations were distinguishable by tissue region. Both vaginal T_{MM} and T_{RM} exhibited similar gene expression patterns as compared with cervical and uterine localized memory CD4 T cells. All FRT CD4 T cells were distanced from dLN T_{CM} and T_{EM}. Together, these data show that the FRT memory CD4 T-cell populations have a distinctive RNA signature based on the site of localization.

Distinct transcriptional profiles of vaginal T_{MM} and T_{RM} are identified in pig-tailed macaques

Although we found that vaginal CD4 T_{MM} and T_{RM} possessed a unique transcriptional profile as compared with T_{RM} in the cervical and uterine regions, differences in the genetic programs of T_{MM} and T_{RM} subsets based upon localization in the vaginal microenvironment had not been explored. Thus, we compared differentially expressed genes (DEGs) of T_{MM} and T_{RM} from the lumen or tissue using CVL and vaginal biopsy collection. First, PCA showed that the tissue-localized T_{MM} and T_{RM} were closely clustered, while luminal T_{MM} and T_{RM} were each distinguishable (Fig. 3A). Comparing the T_{MM}, few DEGs were detected between luminal and tissue-localized populations suggesting that these were similar populations (Fig. 3B). In contrast, the luminal T_{MM} and T_{RM} exhibited greater DEGs, indicating these populations were more transcriptionally distinct (Fig. 3C). Gene Ontology analysis of luminal T_{MM} and T_{RM} identified that T_{MM} were enriched for genes involved in hormonal regulation, cell proliferation, and immune activation (Fig. 3D). Consistent with our previous functional analysis (Fig. 1F and Supplementary Fig. 1), T_{MM} were enriched for genes regulating IL-2 production. In contrast, T_{RM} was enriched for pathways involved in fatty acid transport, consistent with T_{RM}-specific metabolic programs[31]. Together, these data show that within the vaginal tissues, T_{MM} and T_{RM} express largely overlapping transcriptional signatures. However, luminal T_{MM} and T_{RM} differ in the expression of several key genetic programs associated with distinct lineages.

Next, to test whether the menstrual cycle may influence changes in the transcriptional programs of the luminal and tissue-localized vaginal T_{MM} and T_{RM}, we sampled pig-tailed macaques longitudinally at the fertility and luteal phases by using sex swelling characteristics (Fig. 3E)[32]. These comparisons showed that while T_{RM} populations overall exhibited few DEGs, T_{MM} presented with a greater amount of DEGs, most prominently from the luminal T_{MM} populations (Fig. 3F and 3G). Although gene increases from luminal T_{MM} were most likely found at the fertility time points, such as the purinergic DNA damage sensor P2RY13 and the apoptosis signaling molecule DEDD, increased interferon response gene ISG15 and T-cell proliferation gene MKI67 was detected at the luteal phase. Taken together, these data suggest that transcriptionally, the T_{MM} population may undergo changes over the menstrual cycle while the T_{RM} population remains relatively more stable.

CCR5 signaling and vaginal CD4 T-cell populations exhibit fluctuation patterns over the menstrual cycle of pig-tailed Macaques

To better understand how the menstrual cycle might influence the vaginal CD4 T-cell subsets, we performed longitudinal immune profiling (Fig. 4A). Bi-weekly blood samples and weekly CVL samples were collected from six cycling animals over 9 weeks to measure sex hormones, chemokines, and CD4 T-cell properties. P4 and E2 were measured from blood plasma to identify and stratify cycle phases for comparison. First, from blood, we detected an increase in chemokines IP-10, MIP-1α, and MIP-1β specifically within the luteal phase and most likely occurring under conditions of early P4 withdrawal (the late luteal phase) (Fig. 4B). Similar variations in CCR5 expression from circulating memory CD4 T cells were observed, with peak expression identified within the luteal phase prior to P4 withdrawal (Fig. 4C). Comparison of circulating memory CD4 T cells at the follicular or luteal phase using transwell cell migration assays confirmed increased chemotaxis to CCR5-chemokines during the luteal phase (Fig. 4D). Together, these results indicate that during the luteal phase, increased systemic proinflammatory signals are coupled with an increased potential for CCR5-specific trafficking by memory CD4 T cells in circulation. Next, to test whether the vaginal CD4 T-cell subsets display similar fluctuations in CCR5-signaling over the menstrual cycle, we measured CCR5 chemokines in CVL supernatant, along with IL-8, which is produced during the luteal phase of the menstrual cycle in order to facilitate leukocyte recruitment into the endometrium[33]. Both MIP-1β and IL-8 levels were increased during the luteal phase, whereas MIP1a levels were not significantly increased (Fig. 4E). Correlations of IL-8 and both MIP1a and MIP-1β levels identified positive relationships, demonstrating that CCR5 chemokine production corresponded with endometrial remodeling cues (Fig. 4F).

To test whether CCR5 chemokine fluctuations corresponded with changes in vaginal CD4 T cells, we analyzed CVL T cells according to basic cycle phases (Fig. 4G and Supplementary Fig. 2). This showed that CD4 T-cell yields increased during the luteal phase (week 3.0–3.5) and then decreased prior to menstruation onset (week 4.0), remaining at lower levels during the follicular phase (week 4.5). T_{MM} frequencies exhibited similar behavior, increasing at the luteal phase (Fig. 4H), while T_{RM} frequency reciprocally decreased (Fig. 4I). Taken together, these data show consistent and predictable changes in both the circulating and

luminal CD4 T-cell populations in the FRT occur over the menstrual cycle and are correlated with increased CCR5-signaling during the luteal phase.

Oral Maraviroc inhibits T_{MM} migration during the luteal phase in pig-tailed macaques

To determine whether the menstrual cycle dictates migratory FRT T-cell surveillance through CCR5 signaling, we administered an oral CCR5 antagonist drug, Maraviroc (MVC), daily for a course of 5 days in pig-tailed macaques during either the follicular or luteal phase of the menstrual cycle (Fig. 5A). MVC concentrations were detected in FRT secretions (determined from CVL supernatant) on day 5 of treatment at both phases, demonstrating drug penetrance (Fig. 5B). The efficacy of MVC was determined by receptor occupancy assay (Fig. 5C), which confirmed drug action through the reduction in CCR5 internalization from both PBMC CD4 T_{CM} and T_{EM} (Fig. 5D).

Following MVC treatment, no change in the CVL CD4 T-cell yields was observed during the follicular phase; however, a significant decrease in CVL CD4 T cells was detected during the luteal phase (Fig. 5E). By analyzing the change in CVL CD4 T cells following MVC treatment in a multiple linear regression estimation model, we identified that a decrease in CVL CD4 T cells occurred following MVC administration during the luteal phase as compared with the placebo-treated arm (Fig. 5F). Notably, this reduction was specific to the T_{MM} population, whereas no significant difference was estimated with T_{RM} (Fig. 5G). Taken together, these data show that CCR5 antagonism inhibits T_{MM} recruitment into the vaginal lumen during the luteal phase of the menstrual cycle.

DISCUSSION

Genitourinary pathogens, including the causative agents of STIs or as a result of microbiome overgrowth, can lead to severe diseases in women in addition to congenital transmissions. CD4 T cells are essential for optimal immune protection against a variety of genital tract infections, and emerging evidence shows that memory T-cell localization in the FRT may be an important component of vaccine designs aimed at preventing many infections[4,34,35]. Although tissue environments provide critical signaling support required for T-cell localization, survival, and persistence[36], the impact of menstruation on this homeostasis in the FRT remains poorly understood. Here, we report that the FRT T-cell pool is comprised of functionally distinct subsets that undergo oscillating changes in distribution. Notably, localized inflammation associated with tissue remodeling during the luteal phase of the menstrual cycle is associated with a transient shift in CD4 T-cell subset composition at the site of STI pathogen exposure that occurs through CCR5-mediated recruitment. Thus, unlike memory T-cell surveillance within other barrier tissues, the vaginal memory CD4 T-cell pool is in a continual state of fluctuation due to the process of menstruation.

Memory T cells within peripheral tissues are described as primarily comprising T_{RM} that permanently reside in the tissue and T_{EM} that are transiting while conducting immune surveillance[37]. However, a growing number of reports describe an additional memory T-cell subset expressing CCR7, which can traffic through multiple tissue sites in addition to the ability to recirculate[23,38]. Here, we identified that the vaginal mucosa comprises a predominant population of CD4 T cells that are phenotypically consistent

with this population, which we refer to as FRT T_{MM}. While the ontology of FRT T_{MM} and relatedness to the broader memory T-cell subtypes is still an open area of investigation, the variable expression of L-selectin, which, while shown to be consistent with these peripheral migratory T cells in functional studies[22], might also suggest that these populations could comprise T_{CM}. Moreover, the lymphoid trafficking properties and preferential IL2 production by FRT T_{MM} align with T_{CM}[25]; however, intravital labeling with RNA sequencing clearly distinguishes T_{MM} from T_{CM} and instead shows T_{MM} as more transcriptionally similar to T_{RM}. We and others have previously reported that tissue entry can drive substantial transcriptional reprogramming of T cells as they adapt to the local microenvironment[39,40]. Thus, similar transcriptional profiles of FRT subsets could be driven, in part, by tissue co-localization. One interesting area of future investigation will be to determine whether FRT T_{MM} can convert into T_{RM}. Prior studies have shown that T cell ingress into some peripheral tissues, combined with TGF-β receptor signaling, is sufficient to promote T_{RM} differentiation[41]. This raises the possibility that periodic influxes of T_{MM} during the luteal phase alter the repertoire of the FRT CD4 T_{RM} population. As our data also demonstrate FRT T_{MM} surveillance might contribute to cell-mediated protection, it is tempting to speculate that T_{MM} trafficking at this time may be a mechanism to bolster the local antigen-specific T-cell repertoire at a time when tissue remodeling alters epithelial barrier integrity[42].

Artificially modifying lower FRT barrier integrity through high-dose progestin-based contraception such as Medroxyprogesterone acetate (MPA) has been previously shown to increase local CCR5-expressing CD4 T cells[43,44]. While MPA functions display some important differences, our investigation over the menstrual cycle finds that endogenous progesterone production is associated with T_{MM} trafficking into the FRT via CCR5 signaling. Interestingly, we found that T_{MM} are enriched for gene pathways involved in hormonal regulation. As some evidence suggests T cells can both respond to and produce gonadotropin hormones[45,46], T_{MM} may be directly regulated by sex hormones in addition to CCR5-binding chemokines. Nevertheless, blocking CCR5 at the luteal phase of the menstrual cycle prevented T_{MM} recruitment, while no effect on CD4 T_{RM} was detected. Therefore, we demonstrate the essential role of CCR5 signaling in migratory T-cell surveillance of the FRT when local production of CCR5-binding chemokines is increased.

In the context of HIV susceptibility, previous studies show that CCR5 signaling detected in the circulation and from the FRT is correlated to acquisition risk[47,48]. Our findings describe that one potential explanation for this affect is an increased likelihood of HIV target cell trafficking into sites of exposure, including the FRT. Moreover, by using microscopy, combined with intravital labeling and RNA sequencing, we identify T_{MM} not only within the epithelium but also positioned within the underlying vaginal tissues and thus access to the circulation. T_{MM} has been previously demonstrated to undergo recirculation into dLN[23], which might provide a direct route for HIV to access lymphatics from the FRT and establish a systemic infection. Although not shown effective in preventing HIV infection from rectal challenge[49], interestingly, MVC is evidenced to prevent HIV infection from vaginal exposure[50–52]. Importantly, our study finds evidence that blocking CCR5-mediated target cell trafficking through MVC could help prevent HIV transmission from sexual

contact in women as part of a pre-exposure prophylaxis regimen, and this possibility should be further explored.

To conclude, this study identifies that memory CD4 T cells in the FRT are both a heterogeneous and dynamic population under menstrual cycle regulation. These discoveries underscore the critical need for investigations aimed at understanding cellular immune memory surveillance over the menstrual cycle and how this process can impact both immunity and infection risk from genitourinary pathogens in women.

METHODS

Participant description

CVL and blood samples from nine women participating in a study assessing HIV biomarkers at Grady Clinic (Atlanta, Georgia) were used for analysis. Cross-sectional sample collections occurred when participants were not menstruating; the menstrual cycle phase was otherwise not determined in this analysis. Participants were screened for study eligibility, including HIV-negative status (OraQuick swab, OraSure technologies, Bethlehem, PA, USA) and no recent STIs [self-report and later tested by reverse transcription polymerase chain reaction (PCR) described below]. Additional eligibility required that women were aged 18–45 years, exhibiting normal menses (22- to 35-day cycles for at least 3 cycles), not using any hormonal contraception method or intrauterine device for at least 6 months prior, not pregnant for at least 3 months prior, not breastfeeding, and not experiencing symptomatic vaginal infection or genital ulcer disease at screening. Participants did not have a history of loop electrosurgical excision procedure, conization, or cryosurgery in the previous year. Participants were further screened for medical eligibility based on the Centers for Disease Control and Prevention (CDC) medical eligibility criteria for contraceptive use and clinical judgment[53]. Protocols were approved by the Emory University and CDC Institutional Review Boards and the Grady Research Oversight Committee. All participants provided informed consent. Blood was collected in 8 mL sodium citrate-containing CPT™ tubes (BD Biosciences, Franklin Lakes, NJ, USA) and separated into plasma and PBMC by centrifugation. CVL specimens (10 mL collections) were processed as previously described[17]. CVL samples with blood detection (>2% frequency of naïve T cells CCR7 + CD45RA+ from the T-cell population) were excluded from the analysis.

Sexually transmitted infection testing

DNA was extracted from DrySwab® (Lakewood Biochemical Company, Dallas, TX, USA) using the Qiagen DNA Mini kit (Qiagen, Hilden, Germany) and used to amplify targets from *Neisseria gonorrhoeae, Chlamydia trachomatis*, Herpes simplex virus types 1 and 2, *mycoplasma genitalium*, and *Trichomoniasis vaginalis*, using real-time duplex PCR and Qiagen Rotor-Gene Q and 6000 real-time PCR instruments. Qiagen Rotor-Gene Q Series software was used to analyze data.

NHP ethics statement

All of the animal procedures performed in this study were approved by the CDC Institutional Animal Care and Use Committee. Macaques were housed at the CDC under the full care of CDC veterinarians in accordance with the standards incorporated in the *Guide for the Care and Use of Laboratory Animals* (National Research Council of the National Academies, 2010). Macaques in moribund status or reaching Institutional Animal Care and Use Committee-approved endpoints were humanely euthanized in accordance with the American Veterinary Medical Association Guidelines on Euthanasia, June 2007. All procedures were performed under anesthesia using ketamine, and all efforts were made to minimize suffering, improve housing conditions, and provide enrichment opportunities.

NHP specimens

Tissues from three adult female rhesus macaques of reproductive age were used to study a $SHIV_{162P3}$ recall response from CD4 T cells. Animals were challenged rectally with 10TCID50 $SHIV_{162P3}$ weekly until the infection was detected by RT-PCR. SHIV RNA was measured from blood plasma weekly using a modified one-step reverse transcriptase PCR (RT-PCR) method as previously described (15 minutes at 48 °C sensitivity 50 RNA copies/ml)[54]. The estimated time of infection was defined as 7 days prior to the first positive RNA RT-PCR in plasma to account for the eclipse period between virus inoculation and detection of SHIV RNA in plasma.

16 healthy pig-tailed macaques of reproductive age (uninfected with SHIV) were used to investigate FRT T cells and immune properties over the menstrual cycle. For animals administered MVC, drug preparation and administration were carried out as previously described[49]. During time points of MVC treatment, the drug was administered orally by gavage once daily for a course of 5 days.

Intravital labeling

Intravital staining and discrimination in macaques were performed as previously described[55]. Briefly, αCD45 conjugated to R-phycoerythrin (PE) or Biotin (to be followed by *ex vivo* incubation of cells with streptavidin-PE) was diluted into sterile saline and IV injected into the saphenous vein and allowed to circulate for 15 minutes prior tissue collection. For longitudinal sampling, animals were observed for reproductive cycling kinetics by monitoring sex swelling characteristics and menstruation 5 weeks prior to the procedures. Following the initial sampling with αCD45 (clone D058-1283) IV labeling, animals were rested for 6 weeks prior to the second sampling using a recombinant αCD45 for IV labeling.

Microscopy

Tissues were flash-frozen in O.C.T. (optimal cutting temperture) compound by floating on liquid nitrogen. Blocks were sectioned at 7 microns on a cryostat, and slides were fixed in 75:25 acetone/ethanol. The slides were blocked with FACS wash containing 1 μg/ml anti-mouse CD16/32 (clone 2.4G2), 10% mouse serum, 10% rat serum, and 10% donkey serum. Antibodies were from Abcam: rabbit anti-pan cadherin Alexa Fluor® 488 (clone EPR1792Y), rabbit anti-CCR7 Alexa Fluor® 488 (clone Y59), with DAPI staining

solution; BioLegend: anti-mouse TCRα/β-Alexa Fluor® 647 (clone R73). Coverslips with Prolong Gold were applied, and the slides were cured overnight before imaging. Imaging was performed on a Zeiss Axio Observer Z1 with an Axiocam 506 monochromatic camera. Image processing was performed with Zen 2 software.

RNA sequencing

For each population, up to 1000 cells were sorted into RLT lysis buffer (Qiagen, Hilden, Germany) containing 1% BME, and total RNA was purified using the Quick-RNA Microprep kit (Zymo Research, Irving, CA, USA). All resulting RNA was used as an input for complementary DNA synthesis using the SMART-Seq v4 kit (Takara Bio, San Jose, CA, USA) and 10 cycles of PCR amplification. Next, 1 ng cDNA was converted to a sequencing library using the NexteraXT DNA Library Prep Kit and NexteraXT indexing primers (Illumina, San Diege, CA, USA) with ten additional cycles of PCR. Final libraries were pooled at equimolar ratios and sequenced on a HiSeq2500 using 50-bp paired-end sequencing or a NextSeq500 using 75-bp paired-end sequencing. Raw fastq files were mapped to the MacamM v7 build of the Rhesus macaque genome[56] using STAR[57] with the v7.8.2. transcriptome annotation library reference transcriptome. PCR duplicate reads were flagged with PICARD mark duplicates and excluded from downstream analyses. The overlap of reads with exons was computed and summarized using the GenomicRanges[58] package in R/Bioconductor, and data was normalized to fragments per kilobase per million. Genes that were expressed at a minimum of three reads per million in all samples for each cell typed were considered to be expressed. DEGs were determined using the glm function in edgeR[59] using the animal from which each cell type originated as a covariate. Genes with a false discovery rate (FDR) < 0.05 and absolute log2(FC) > 1 were considered to be significant. Gene Ontology analysis was performed from DEGs as previously described[39]. All code for data processing and display is available upon request.

NHP tissue specimen processing

Human and NHP blood and CVL samples were processed similarly. FRT tissues were processed into single-cell suspensions using collagenase type II (62.5 U/ml) and DNase I (0.083 U/ml) (STEMCELL Technologies, Vancouver, Canada) and separated by Percoll (GE Healthcare Life Sciences, Chicago, Illinois, USA) density centrifugation. Enriched leukocytes were washed and resuspended in cell media for phenotyping or functional assays.

Sex-hormone measurement and estimating menstrual cycle phase

Plasma P4 and E2 were quantified by immunoassay as one batch. Assay services were provided by the Biomarkers Core Laboratory at the Yerkes National Primate Research Center. Menstrual cycle phase was estimated by P4 and E2 kinetics relative to a 32-day menstrual cycle (average length of pigtail macaque menstrual cycle) and by observed menstruation.

Soluble cytokine/chemokine measurement

CVL supernatant and blood plasma were measured and analyzed for cytokines/chemokines through the Emory Multiplexed Immunoassay Core using the Meso Scale Discovery

platform (Meso Scale, Rockville, MD, USA) with an NHP multiplex assay kit in one batch run.

MVC drug measurement

MVC concentrations in mucosal secretions were measured by high-performance liquid chromatography-mass spectrometry/mass spectrometry (MS/MS) (Shimadzu Scientific, SCIEX, Columbia, Maryland, USA). Briefly, MVC was extracted from Weck-Cel surgical spears (Beaver-Visitec International, Inc., Waltham, Massachusetts, USA) used to collect vaginal secretions (~25 μl), using 500 μl of methanol containing internal standard [deuterium-labeled MVC (MVC-d6); Toronto Research Chemicals, Toronto, Canada]. After centrifugation, the extracted liquid was evaporated and resuspended in 150 μl of mobile phase A (0.2% formic acid in water). 10 μl of final solution was injected into a UK-C18 column (1 × 100 mm; Imtakt, Portland, Oregon, USA) connected to the high-performance liquid chromatography-MS/MS system. Aqueous-acetonitrile mobile-phase gradient was used to elute MVC from the column into the MS/MS system. MVC mass transitions (*m/z*) of 514.1/117.2 and 514.1/389.5 were monitored in positive MRM mode. MVC concentrations were calculated using Analyst software (SCIEX, Columbia, Maryland, USA) from a standard curve with a dynamic range of 1–2000 ng/ml. The lower limit of quantification was 5 ng/ml.

Analysis of MVC binding to CCR5 by a MIP-1β internalization assay

MVC binding to CCR5 was determined *ex vivo* using the MIP-1β internalization assay as previously described[49]. In brief, 1×10^6 PMBCs were incubated with 20 ng of MIP-1β (recombinant human CCL4/MIP-1β isoform LAG-1; R&D Systems, Minneapolis, Minnesota, USA) for 30 minutes at 37 °C. Cell surface CCR5 receptors are internalized upon binding to MIP-1β (a natural ligand of CCR5), and MVC binding to CCR5 prevents internalization by MIP-1β, allowing extracellular CCR5 measurement by flow cytometry.

Statistical analysis

Generalized estimating equations—In the event of comparisons with repeated measures, models used to compare cellular immune markers and levels of soluble inflammatory cytokines concentrations by cycle phase were fit using generalized estimating equations with an exchangeable working correlation structure.

Regression modeling—Correlations of IL-8 with CCR5 chemokines in macaques were evaluated by generalized multivariate regression modeling to adjust for the subject effect followed by the calculation of Pearson correlation coefficients on the residuals. Regression model for cellular characteristics following oral MVC administration in macaques.

$$Y = BO + B1\,(MVC) + B2\,(luteal) + B3\,(MVC) * (luteal)$$

Prism 5 software (GraphPad Software, San Diego, California) was otherwise used to determine statistical significance from mean comparisons. Multiple comparisons were corrected using the FDR.

Intracellular cytokine staining

Cells in media with 20U/ml IL-2 (Roche, Basel, Switzerland) were activated with Cell Stimulation Cocktail (Affymetrix eBioscience, San Diego, California, USA) or overlapping $SHIV_{162P3}$ envelope peptides for 5 hours (AIDS Research and Reference Reagent Program, Division of AIDS, National Institute of Allergy and Infectious Diseases, National Institutes of Health). Following surface staining, cells were permeabilized using a Cytofix/Cytoperm kit as recommended by the manufacturer (BD Biosciences, Franklin Lakes, New Jersey, USA) prior to intracellular antibody staining. Background values from matched untreated populations were subtracted from cytokine measurements.

Cell staining and flow cytometry

Cell viability was determined using the Zombie Fixable Viability Kit (Biolegend®, San Diego, California, USA) then incubated with anti-CD16/32 Fc block (BioXcell, Lebanon, New Hampshire, USA). Cells were measured using an LSRII flow cytometer or mechanically sorted using a Sony SH800. Flow data was acquired using FACS DIVA software (BD Biosciences, Franklin Lakes, New Jersey, USA) and analyzed using FlowJo software (TreeStar, Inc., Ashland, Oregon, USA). For cell sorting, viable lymphocyte-gated singlet cells were discriminated for IV-CD45 (PE) negative and CD45+ (BV450) followed by CD3+ and CD4+. Next, CD45RA− CD4 T cells were sorted by CCR7 expression. The following fluorochrome-conjugated antibodies were used in this study:

Human antibodies

antibody	conjugate	clone	vendor
CD3	Brilliant Violet 421™	UCHT1	Biolegend®
CD4	Alexa Fluor® 700	RPA-T4	BD Biosciences
CD4	Brilliant Violet 785™	RPA-T4	Biolegend®
CD8a	Brilliant Violet 510™	RPA-T8	Biolegend®
CD45	APC/FIRE™750	2D1	Biolegend®
CD45RA	Brilliant Violet 605™	HI100	Biolegend®
CCR7	PE-CF594	150,503	BD Biosciences
CXCR3	PerCp/Cyanine5.5	G025H7	Biolegend®
CX3CR1	PerCp-eFlour®780	2A9-1	affymetrix eBioscience
CCR4	PerCP/Cyanine5.5	IG1	Biolegend®
CCR5	PE	3A9	BD Biosciences
CCR6	Brilliant Violet 605™	G034E3	Biolegend®
CCR9	APC	L053E8	Biolegend®
α4β7	conjugated to APC (Molecular probes)		NIH AIDS reagent program
IFNγ	APC	25723.11	BD Biosciences
IL-2	Brilliant Violet 605™	MQ1-17H12	BD Biosciences
TNFα	Brilliant Violet 711™	Mab11	Biolegend®
IL-17A	PE	N49-653	BD Biosciences

antibody	conjugate	clone	vendor
IL-10	PerCP/Cyanine5.5	JES3-9D7	Biolegend®
CD62P	PerCp-eFlour®780	Psel. KO2.3	affymetrix eBioscience
CD62L	Brilliant Violet 650™	DREG-56	Biolegend®
CD66b	APC	G10F5	BD Biosciences
CD69	Brilliant Violet 650™	FN50	Biolegend®
CD103	Fluorescein isothiocyanate (FITC)	Ber-ACT8	BD Biosciences

NHP antibodies

antibody	conjugate	clone	vendor
CD3	Alexa Fluor® 700	SP34-2	BD Biosciences
CD4	Brilliant Violet 785™	OKT4	Biolegend®
CD4	FITC	OKT4	Biolegend®
CD8	V500	RPA-T8	BD Biosciences
CD45	BD Horizon™ BV450	D058-1283	BD Biosciences
CD45	Biotin or PE	D058-1283	BD Biosciences
CD45	Biotin	REA1023	Miltenyi Biotec
CD45RA	PE-Cy™7	5H9	BD Biosciences
CCR5	PE	3A9	BD Biosciences
CCR7	PE-CF594	150,503	BD Biosciences
CCR7	Alexa Fluor® 647	150,503	BD Biosciences
IFNγ	APC	B27	BD Biosciences
IL-2	PE-Cy™7	MQ1-17H12	BD Biosciences
TNFα	FITC	Mab11	BD Biosciences

Supplementary Material

Refer to Web version on PubMed Central for supplementary material.

ACKNOWLEDGMENTS

We thank the study participants and colleagues who contributed to the clinical studies. From the CDC we thank Ivana Massud, Jim Smith, Sunita Sharma, Susan Rhone, Amy Martin, Mian-er Cong, & Kenji Nishiura for assistance with NHP studies, Cheng-Yen Chen, and Kathryn A. Lupoli for STI testing in human samples, Jillian Condrey, James Mitchell, Shanon Ellis, Frank Deyounks, Kristen Kelley for animal technical assistance, and Dr. David Garber for programmatic support.

FUNDING

This study was supported by the U.S. Centers for Disease Control and Prevention, Atlanta, GA 30329, and Emory University and in part by NIH grants R35HL150803 (J.E.K) and U01HL139483 (R.A. and J.E.K.), K23AI114407 (A.N.S), K23HD078153-01A1 (L.B.H), the Emory University Center for AIDS Research (P30AI050409), the Atlanta Clinical and Translational Sciences Institute (KLR2TR000455, UL1TR000454), and the Biomarker Core Laboratory at the Yerkes National Primate Research Center Base Grant P51OD011132. This study was supported in part by the Emory Multiplexed Immunoassay Core (EMIC), which is subsidized by the Emory University School of Medicine and is one of the Emory Integrated Core Facilities. Additional support was provided by the National

Center for Georgia Clinical & Translational Science Alliance of the National Institutes of Health under Award Number UL1TR002378.

References

1. Shin H & Iwasaki A A vaccine strategy that protects against genital herpes by establishing local memory T cells. Nature 491, 463–467 (2012). [PubMed: 23075848]
2. Stary G et al. Vaccines. A mucosal vaccine against Chlamydia trachomatis generates two waves of protective memory T cells. Science 348, aaa8205 (2015). [PubMed: 26089520]
3. Li Z et al. Novel vaccination protocol with two live mucosal vectors elicits strong cell-mediated immunity in the vagina and protects against vaginal virus challenge. J. Immunol. 180, 2504–2513 (2008). [PubMed: 18250460]
4. Poston TB, Gottlieb SL & Darville T Status of vaccine research and development of vaccines for Chlamydia trachomatis infection. Vaccine 37, 7289–7294 (2019). [PubMed: 28111145]
5. Iijima N & Iwasaki A T cell memory. A local macrophage chemokine network sustains protective tissue-resident memory CD4 T cells. Science 346, 93–98 (2014). [PubMed: 25170048]
6. Xu H, Wang X & Veazey RS Mucosal immunology of HIV infection. Immunol. Rev. 254, 10–33 (2013). [PubMed: 23772612]
7. Olive AJ, Gondek DC & Starnbach MN CXCR3 and CCR5 are both required for T cell-mediated protection against C. trachomatis infection in the murine genital mucosa. Mucosal Immunol. 4, 208–216 (2011). [PubMed: 20844481]
8. Davila SJ, Olive AJ & Starnbach MN Integrin α4β1 is necessary for CD4+ T cell-mediated protection against genital Chlamydia trachomatis infection. J. Immunol. 192, 4284–4293 (2014). [PubMed: 24659687]
9. Beura LK et al. CD4+ resident memory T cells dominate immunosurveillance and orchestrate local recall responses. J. Exp. Med. 216, 1214–1229 (2019). [PubMed: 30923043]
10. Iijima N & Iwasaki A Tissue instruction for migration and retention of TRM cells. Trends Immunol. 36, 556–564 (2015). [PubMed: 26282885]
11. Forcey DS et al. Chlamydia detection during the menstrual cycle: a cross-sectional study of women attending a sexual health service. PLoS One 9, e85263 (2014). [PubMed: 24475042]
12. Rice PA, Shafer WM, Ram S & Jerse AE Neisseria gonorrhoeae: drug Resistance, Mouse Models, and Vaccine Development. Annu. Rev. Microbiol. 71, 665–686 (2017). [PubMed: 28886683]
13. Swaims-Kohlmeier A et al. Proinflammatory oscillations over the menstrual cycle drives bystander CD4 T cell recruitment and SHIV susceptibility from vaginal challenge. EBioMedicine 69, 103472 (2021). [PubMed: 34229275]
14. Catalini L & Fedder J Characteristics of the endometrium in menstruating species: lessons learned from the animal kingdom†. Biol. Reprod. 102, 1160–1169 (2020). [PubMed: 32129461]
15. Wira CR, Rodriguez-Garcia M & Patel MV The role of sex hormones in immune protection of the female reproductive tract. Nat. Rev. Immunol. 15, 217–230 (2015). [PubMed: 25743222]
16. United Nations. Contraceptive use by method 2019. Available at: https://www.un.org/development/desa/pd/sites/www.un.org.development.desa.pd/files/files/documents/2020/Jan/un_2019_contraceptiveusebymethod_databooklet.pdf [Date accessed: XXX].
17. Swaims-Kohlmeier A et al. Progesterone levels associate with a novel population of CCR5+CD38+ CD4 T cells resident in the Genital mucosa with lymphoid trafficking potential. J. Immunol. 197, 368–376 (2016). [PubMed: 27233960]
18. Duluc D et al. Functional diversity of human vaginal APC subsets in directing T-cell responses. Mucosal Immunol. 6, 626–638 (2013). [PubMed: 23131784]
19. McKinnon LR et al. Characterization of a human cervical CD4+ T cell subset coexpressing multiple markers of HIV susceptibility. J. Immunol. 187, 6032–6042 (2011). [PubMed: 22048765]
20. Rodriguez-Garcia M, Barr FD, Crist SG, Fahey JV & Wira CR Phenotype and susceptibility to HIV infection of CD4+ Th17 cells in the human female reproductive tract. Mucosal Immunol. 7, 1375–1385 (2014). [PubMed: 24759207]

21. Staumont-Sallé D et al. CX3CL1 (fractalkine) and its receptor CX3CR1 regulate atopic dermatitis by controlling effector T cell retention in inflamed skin. J. Exp. Med. 211, 1185–1196 (2014). [PubMed: 24821910]
22. Jameson SC & Masopust D Understanding subset diversity in T cell memory. Immunity 48, 214–226 (2018). [PubMed: 29466754]
23. Bromley SK, Yan S, Tomura M, Kanagawa O & Luster AD Recirculating memory T cells are a unique subset of CD4+ T cells with a distinct phenotype and migratory pattern. J. Immunol. 190, 970–976 (2013). [PubMed: 23255361]
24. Vieira Braga FA et al. A cellular census of human lungs identifies novel cell states in health and in asthma. Nat. Med. 25, 1153–1163 (2019). [PubMed: 31209336]
25. Matos TR et al. Central memory T cells are the most effective precursors of resident memory T cells in human skin. Sci. Immunol 7, eabn1889 (2022). [PubMed: 35452256]
26. Sheridan BS & Lefrançois L Regional and mucosal memory T cells. Nat. Immunol. 12, 485–491 (2011). [PubMed: 21739671]
27. Nakanishi Y, Lu B, Gerard C & Iwasaki A CD8(+) T lymphocyte mobilization to virus-infected tissue requires CD4(+) T-cell help. Nature 462, 510–513 (2009). [PubMed: 19898495]
28. Gebhardt T et al. Memory T cells in nonlymphoid tissue that provide enhanced local immunity during infection with herpes simplex virus. Nat. Immunol. 10, 524–530 (2009). [PubMed: 19305395]
29. Otten RA et al. Multiple vaginal exposures to low doses of R5 simian-human immunodeficiency virus: strategy to study HIV preclinical interventions in nonhuman primates. J Infect Dis 191, 164–173 (2005). [PubMed: 15609225]
30. Schenkel JM & Masopust D Tissue-resident memory T cells. Immunity 41, 886–897 (2014). [PubMed: 25526304]
31. Pan Y et al. Survival of tissue-resident memory T cells requires exogenous lipid uptake and metabolism. Nature 543, 252–256 (2017). [PubMed: 28219080]
32. Bullock DW, Paris CA & Goy RW Sexual behaviour, swelling of the sex skin and plasma progesterone in the pigtail macaque. J. Reprod. Fertil. 31, 225–236 (1972). [PubMed: 4629264]
33. Jabbour HN, Kelly RW, Fraser HM & Critchley HO Endocrine regulation of menstruation. Endocr. Rev. 27, 17–46 (2006). [PubMed: 16160098]
34. Muruganandah V, Sathkumara HD, Navarro S & Kupz A A systematic review: the role of resident memory T cells in infectious diseases and their relevance for vaccine development. Front. Immunol. 9, 1574 (2018). [PubMed: 30038624]
35. Furuta A et al. Bacterial and host determinants of Group B streptococcal infection of the neonate and infant. Front. Microbiol 13, 820365 (2022). [PubMed: 35265059]
36. Mueller SN & Mackay LK Tissue-resident memory T cells: local specialists in immune defence. Nat. Rev. Immunol. 16, 79–89 (2016). [PubMed: 26688350]
37. Woodland DL & Kohlmeier JE Migration, maintenance and recall of memory T cells in peripheral tissues. Nat. Rev. Immunol. 9, 153–161 (2009). [PubMed: 19240755]
38. Watanabe R et al. Human skin is protected by four functionally and phenotypically discrete populations of resident and recirculating memory T cells. Sci. Transl. Med. 7, 279ra39 (2015).
39. Hayward SL et al. Environmental cues regulate epigenetic reprogramming of airway-resident memory CD8+ T cells. Nat. Immunol. 21, 309–320 (2020). [PubMed: 31953534]
40. Crowl JT et al. Tissue-resident memory CD8+ T cells possess unique transcriptional, epigenetic and functional adaptations to different tissue environments. Nat. Immunol. 23, 1121–1131 (2022). [PubMed: 35761084]
41. Mackay LK et al. The developmental pathway for CD103(+)CD8+ tissue-resident memory T cells of skin. Nat. Immunol. 14, 1294–1301 (2013). [PubMed: 24162776]
42. Takamura S Niches for the long-term maintenance of tissue-resident memory T cells. Front. Immunol. 9, 1214 (2018). [PubMed: 29904388]
43. Hapgood JP, Kaushic C & Hel Z Hormonal contraception and HIV-1 acquisition: biological mechanisms. Endocr. Rev. 39, 36–78 (2018). [PubMed: 29309550]

44. Wessels JM et al. Depot medroxyprogesterone acetate (DMPA) enhances susceptibility and increases the window of vulnerability to HIV-1 in humanized mice. Sci. Rep. 11, 3894 (2021). [PubMed: 33594113]
45. Lentz LS et al. Human chorionic gonadotropin promotes murine Treg cells and restricts pregnancy-harmful proinflammatory Th17 responses. Front. Immunol. 13, 989247 (2022). [PubMed: 36203576]
46. Chen A et al. The neuropeptides GnRH-II and GnRH-I are produced by human T cells and trigger laminin receptor gene expression, adhesion, chemotaxis and homing to specific organs. Nat. Med. 8, 1421–1426 (2002). [PubMed: 12447356]
47. Jaumdally SZ et al. CCR5 expression, haplotype and immune activation in protection from infection in HIV-exposed uninfected individuals in HIV-serodiscordant relationships. Immunology 151, 464–473 (2017). [PubMed: 28398593]
48. Liebenberg LJ et al. Genital-systemic chemokine gradients and the risk of HIV acquisition in women. J. Acquir. Immune Defic. Syndr. 74, 318–325 (2017). [PubMed: 28187085]
49. Massud I et al. Lack of prophylactic efficacy of oral maraviroc in macaques despite high drug concentrations in rectal tissues. J. Virol. 87, 8952–8961 (2013). [PubMed: 23740994]
50. Gulick RM et al. Safety and tolerability of maraviroc-containing regimens to prevent HIV infection in women: a phase 2 randomized trial. Ann. Intern. Med. 167, 384–393 (2017). [PubMed: 28828489]
51. Neff CP, Kurisu T, Ndolo T, Fox K & Akkina R A topical microbicide gel formulation of CCR5 antagonist maraviroc prevents HIV-1 vaginal transmission in humanized RAG-hu mice. PLoS One 6, e20209 (2011). [PubMed: 21673796]
52. Neff CP, Ndolo T, Tandon A, Habu Y & Akkina R Oral pre-exposure prophylaxis by anti-retrovirals raltegravir and maraviroc protects against HIV-1 vaginal transmission in a humanized mouse model. PLoS One 5, e15257 (2010). [PubMed: 21203568]
53. Curtis KM et al. U.S. Medical eligibility criteria for contraceptive use, 2016. MMWR Recomm. Rep. 65, 1–103 (2016).
54. Cong ME, Pau CP, Heneine W & García-Lerma JG Antiretroviral drug activity in macaques infected during pre-exposure prophylaxis has a transient effect on cell-associated SHIV DNA reservoirs. PLoS One 11, e0164821 (2016). [PubMed: 27806064]
55. Kauffman KD et al. Defective positioning in granulomas but not lung-homing limits CD4 T-cell interactions with Mycobacterium tuberculosis-infected macrophages in rhesus macaques. Mucosal Immunol. 11, 462–473 (2018). [PubMed: 28745326]
56. Zimin AV et al. A new rhesus macaque assembly and annotation for next-generation sequencing analyses. Biol. Direct 9, 20 (2014). [PubMed: 25319552]
57. Dobin A et al. STAR: ultrafast universal RNA-seq aligner. Bioinformatics 29, 15–21 (2013). [PubMed: 23104886]
58. Lawrence M et al. Software for computing and annotating genomic ranges. PLoS Comput. Biol. 9, e1003118 (2013). [PubMed: 23950696]
59. Robinson MD, McCarthy DJ & Smyth GK edgeR: a Bioconductor package for differential expression analysis of digital gene expression data. Bioinformatics 26, 139–140 (2010). [PubMed: 19910308]

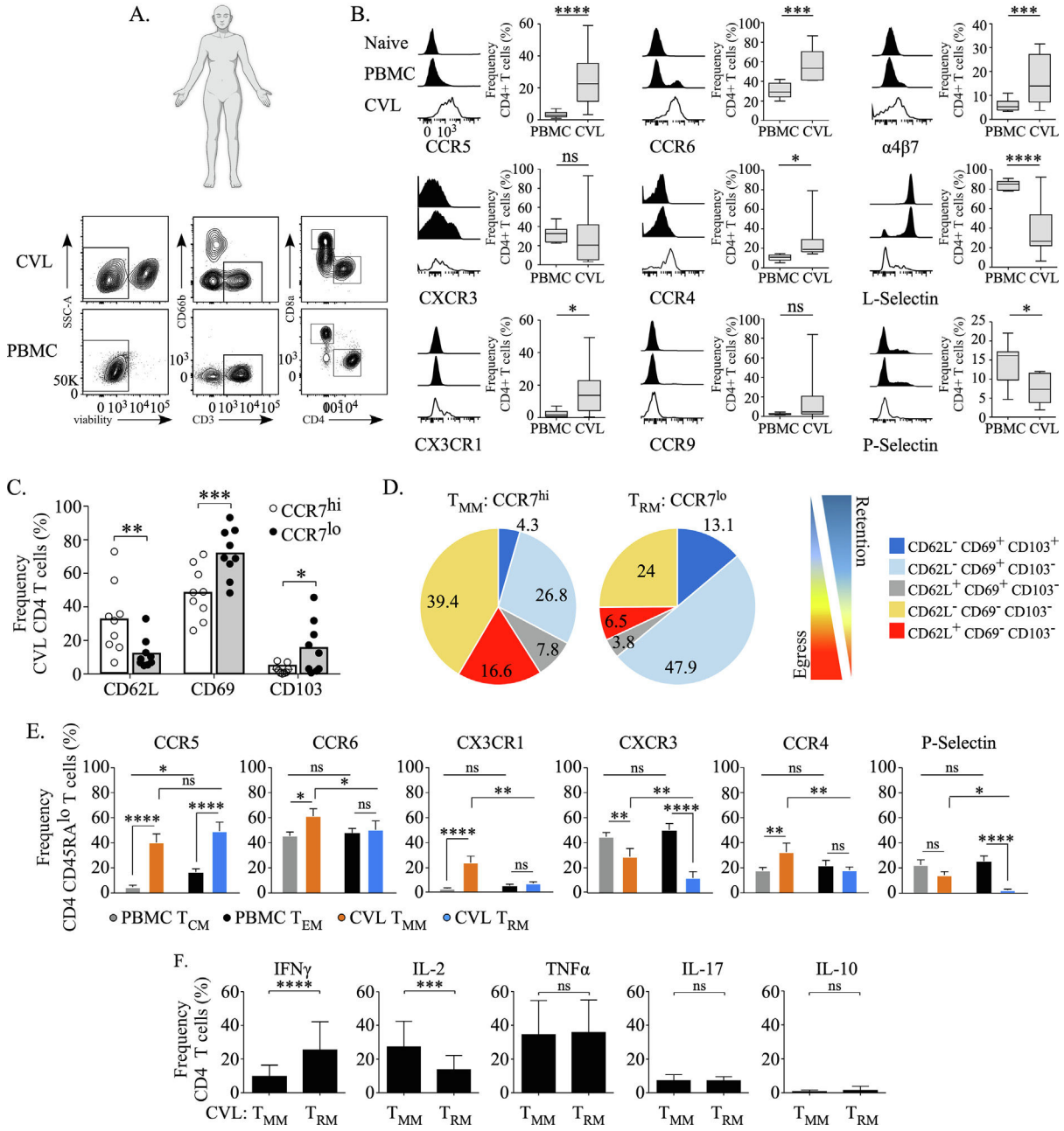

Fig. 1.

Distinct CD4 T-cell populations from human CVL are identified by migratory properties. (A) (Top) profile of the female human form created using BioRender.com. (Bottom) representative gating strategy for CD4 T-cell discrimination from CVL (top panels) and matched-PBMC (bottom panels). Viable, singlet lymphocytes are gated to distinguish T cells from granulocytes (CD66b) prior to CD4 gating. (B) The measurement of indicated chemokine receptors and integrins from CD4 T cells. (Left representative histograms) shown for perspective, (top histogram) naïve gated (CCR7hi CD45RAhi) PBMC CD4 T cells, (center histogram black) total PBMC CD4 T cells, and (bottom histogram white) CVL CD4 T cells. (Right box and whiskers graphs) the expression frequency of chemokine receptors or

integrins from CD4 T cells using naïve PBMC to set gating parameters (N = 9 per group). (C) CD62L, CD69, and CD103 frequency from CVL CCR7hi CD4 T cells (T_{MM}; white dots) and CCR7lo CD4 T cells (T_{RM}; black dots). Shown as a scatter plot graph with bar mean line. (D) Boolean pie charts of CD62L, CD69, and CD103 co-expression from CD4 T_{MM} or T_{RM} measured from (C). (E) The frequency of indicated chemokine receptors and P-Selectin from T_{MM} and T_{RM} compared with matched-PBMC T_{CM} and $T_{EM.}$ (F) The frequency of IFNγ, IL-2, TNFα, IL-17A, and IL-10 production measured from CVL T_{MM} and T_{RM} (N = 9, graph depicted as a column plot with error bar). (B, C, E, and F) Models evaluating a comparison of means were fit using multiple comparisons. The *p* values with the false discovery rate (FDR or *q* value) ≤ 0.05 are shown. (N = 9 per group, data depicted as a bar graph with SEM). *$p \leq 0.05$, **$p < 0.01$, ***$p < 0.001$, ****$p < 0.0001$. CD = clusters of differentiation; CVL = cervicovaginal lavage; IFN = interferon; IL = Interleukin; PBMC = peripheral blood mononuclear cells; T_{CM} = central memory CD4 T cells; T_{EM} = effector memory CD4 T cells; T_{MM} = migratory memory T cell; TNFα = tumor necrosis factor α; T_{RM} = resident memory T cells.

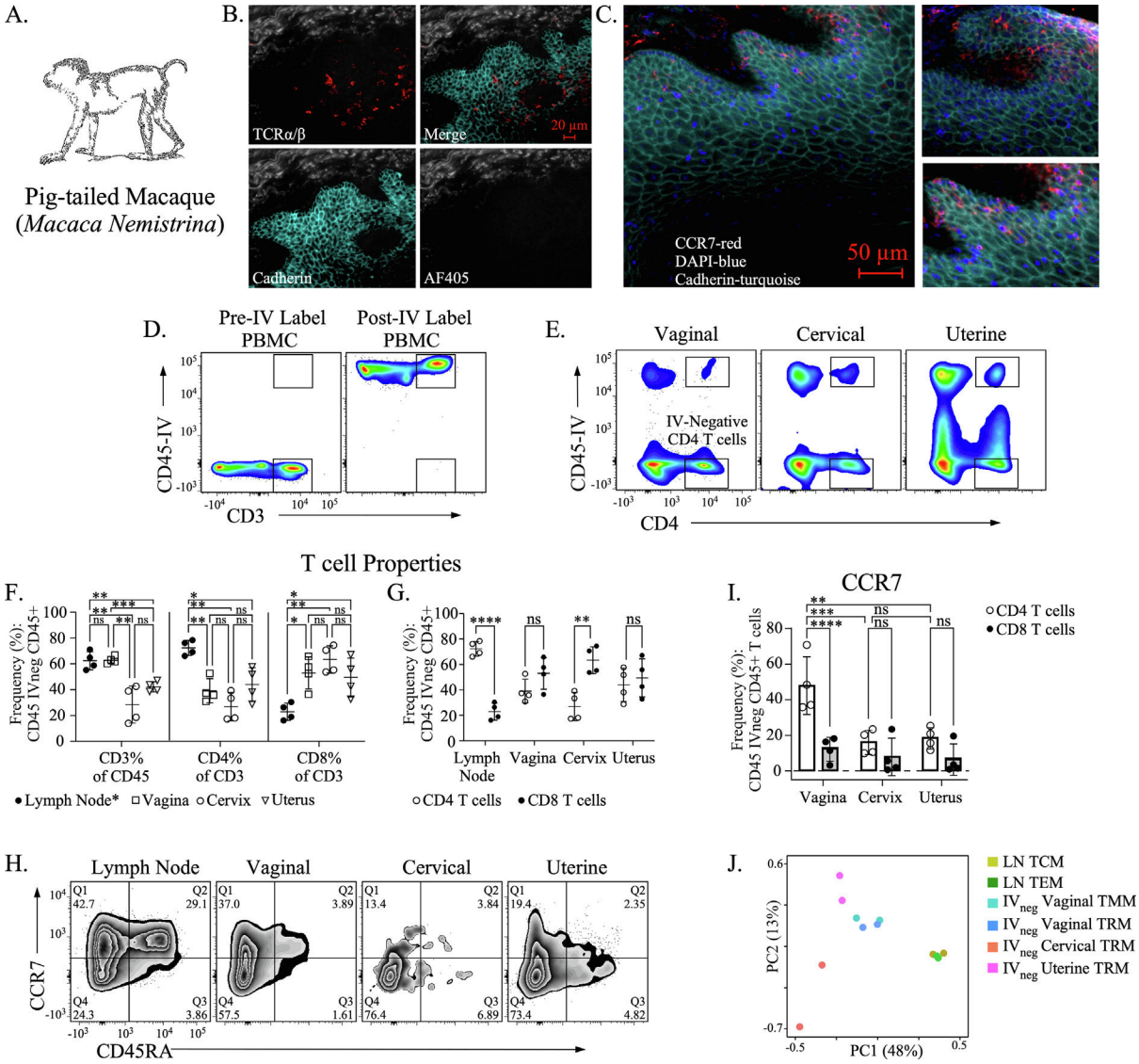

Fig. 2.

CD4 T-cell characterization throughout the FRT. (A) Cartoon depiction of a pig-tailed macaque. (B, C) Fluorescence microscopy imaging of T cells localized in the vaginal epithelium of pig-tailed macaques. T cells are identified by TCRα/β (B) and CCR7 (C). Epithelial cells are identified by cadherin. (D) Flow cytometry plots depicting T cells prior to (left panel) and following IV administration of αCD45 (right panel). (E) Representative cell flow plots depicting IV discrimination of CD4 T cells from FRT tissue compartments. (F, G) Scatter dot plot graphs with mean lines comparing the T cell frequency of lymphocytes or leukocytes (F), or CD4 and CD8 T-cell ratios (G) from the draining lymph nodes (*lymph node cells were not gated by IV discrimination), vagina, cervix, or uterus. (H) Representative cell gating plots for discriminating IV negative memory CD4 T-cell subsets by expression of CD45RA and CCR7 by FRT tissue site. (I) Scatter dot plot graphs with mean line comparing CCR7 expression from memory CD4 and CD8 T cells by FRT tissue. (J) PCA plots of mechanically sorted IV negative memory CD4 T cells (lymph

node T cells were not gated by IV discrimination) from indicated FRT tissues and memory CD4 T cells from the dLN following RNA-seq. Memory CD4 T cells (CD45Alo) were sorted for CCR7 expression. (F, G, I). Models evaluating a comparison of means were fit using multiple comparisons. The p values with a q value ≤ 0.05 are shown. (N = 4) *$p \leq$ 0.05, **$p < 0.01$, ***$p < 0.001$, ****$p < 0.0001$. CD = clusters of differentiation; dLN = draining lymph nodes; RNA-seq = RNA sequencing.

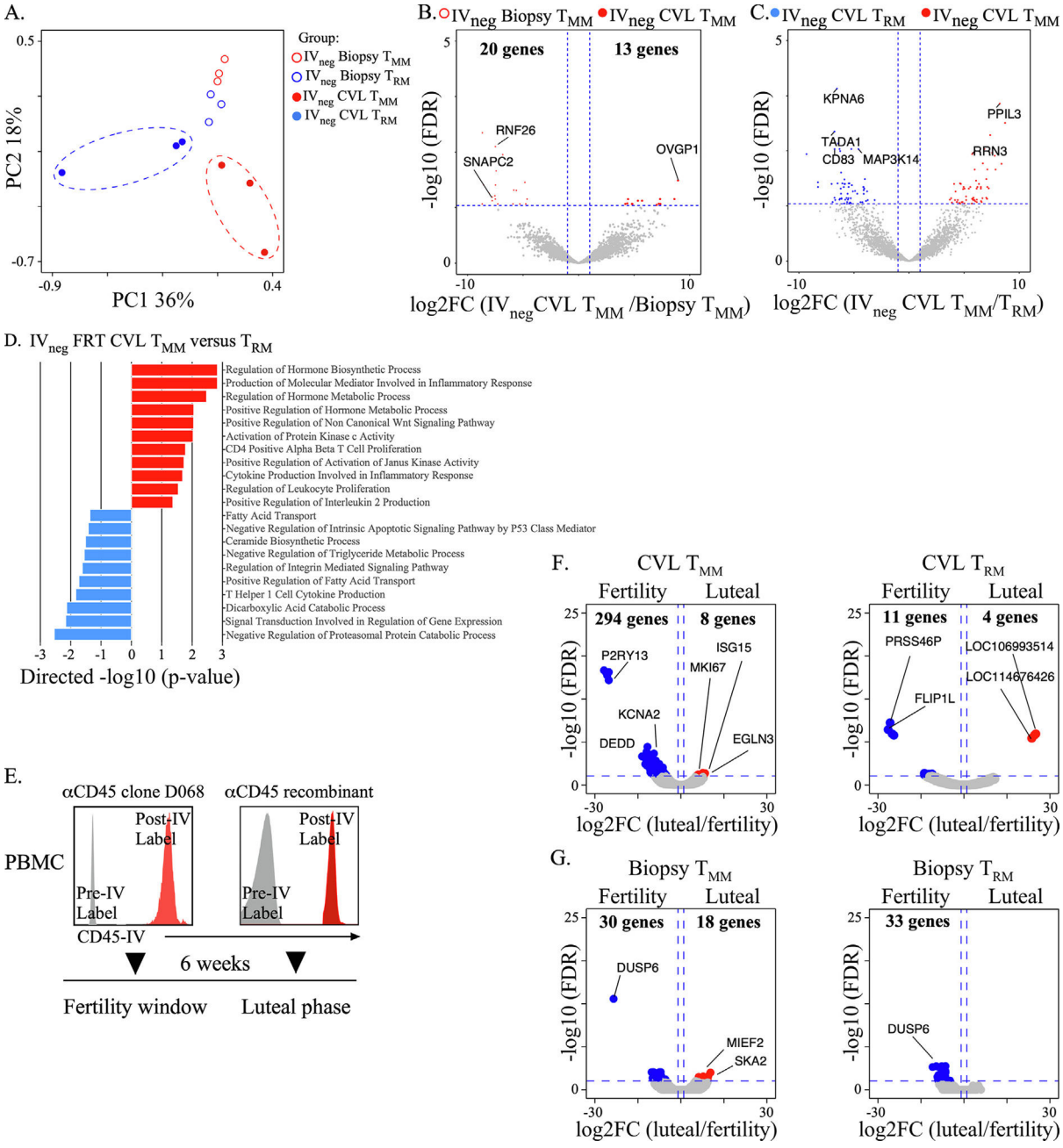

Fig. 3.

Distinct transcriptional profiles of lower FRT T_{MM} and T_{RM}. (A) PCA plots of mechanically sorted IV negative vaginal memory CD4 T-cell populations from pig-tailed macaques following RNA-seq. (B) Volcano plot showing the log2 fold change in gene expression versus the −log10 of the p value for CVL collected T_{MM} versus Biopsy collected T_{MM}, or (C) CVL collected T_{RM} versus CVL collected T_{MM}. (D) Gene Ontology (GO) pathway analysis in T_{MM} versus T_{RM}. The *p* value of each comparison is noted. (E) Schematic and histogram flow plots depicting the IV labeling approach for longitudinal CVL and biopsy sampling in pig-tailed macaques at fertility time points followed by collection at luteal time points 6 weeks later (n = 2). (F) Volcano plots showing the log2 fold change

in gene expression versus the − log10 of the *p* value comparing collections during the fertility and luteal time points for CVL collected T_{MM} (left panel) and CVL collected T_{RM} (right panel) or (G) biopsy T_{MM} (left panel) and biopsy T_{RM} (right panel). CD = clusters of differentiation; CVL = cervicovaginal lavage; FRT = female reproductive tract; PCA = Principal component analysis; T_{CM} = central memory CD4 T cells; T_{MM} = migratory memory T cell; T_{RM} = resident memory T cells.

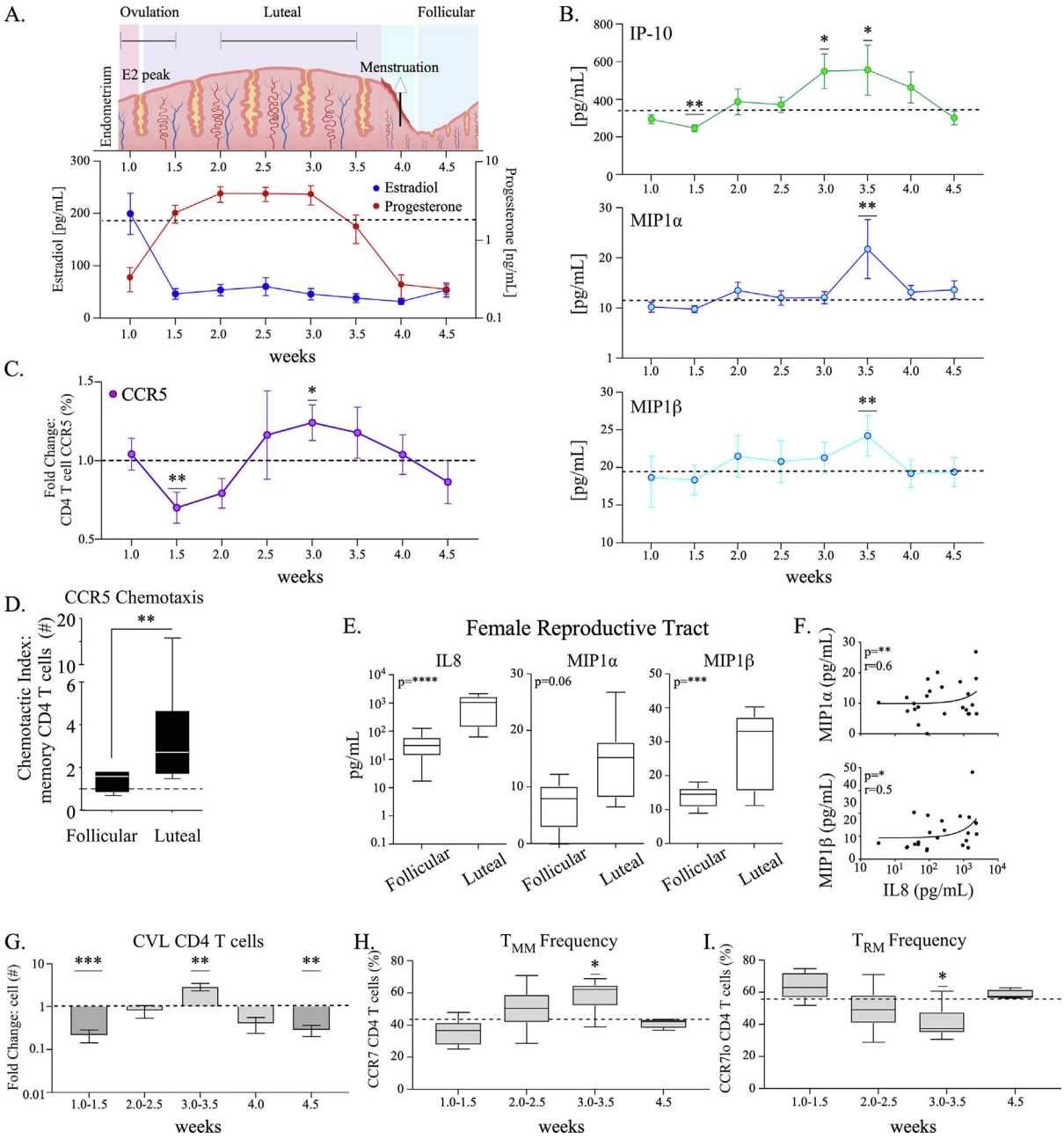

Fig. 4.

Systemic Th1-specific activation and FRT T_{MM} fluctuations occur over the menstrual cycle. (A) (Top) cartoon depiction of endometrial changes occurring over the menstrual cycle of pig-tailed macaques are labeled with the corresponding cycle phase and week starting at the time of ovulation (week 1.0). Created using BioRender.com. (Bottom) A mean line graph with SEM of P4 and E2 measured bi-weekly from six pigtail macaques is stratified by phase of the cycle starting at the time of ovulation (determined by E2 peaks and referenced to the cycle phase). The mean P4 levels are indicated by a dotted line for reference (B) A mean line graph with SEM of indicated cytokine/chemokine concentrations measured longitudinally from blood plasma is plotted over the cycle with the median

value indicated by a dotted line. (C) The fold change in cell surface CCR5 memory CD4 T-cell expression plotted over the cycle. (D) CCR5 chemotaxis from PBMC CD4 T cells collected at the follicular or luteal phase of the cycle is measured by trans-well assay. Shown as a box and whiskers plot, the dotted line represents a chemotactic index of 1 (no net change). Comparisons evaluated by Mann-Whitney test. (E) The concentration of IL-8, Mip1α, and Mip1β detected from CVL at the follicular or luteal phase of the menstrual cycle. (F) An XY graph depicting the concentrations of IL-8 with Mip1α (top panel) or Mip1β (bottom panel). Correlations were evaluated by generalized multivariate regression modeling. Pearson correlation coefficients (r value) and p values (if ≤ 0.05) are shown. (G) A bar graph with SEM depicting the fold change in CVL CD4 T-cell yields over the cycle. Week 4.0 plots include two samples collected prior to the detection of menstruation onset. (H) The frequency of T_{MM} and (I) T_{RM} measured from CVL CD4 T cells over the cycle is shown as a box and whiskers graph. Samples collected during the time frame of menstruation (week 4.0) are excluded. (B, C, G–I) Comparisons were evaluated with a Wilcoxon matched-pairs signed-rank test. (C–I). *$p \leq 0.05$, **$p < 0.01$, ***$p < 0.001$, ****$p < 0.0001$. CD = clusters of differentiation; CVL = cervicovaginal lavage; E2 = estradiol; IL = Interleukin; P4 = progesterone; SEM = standard error of mean; T_{MM} = migratory memory T cell.

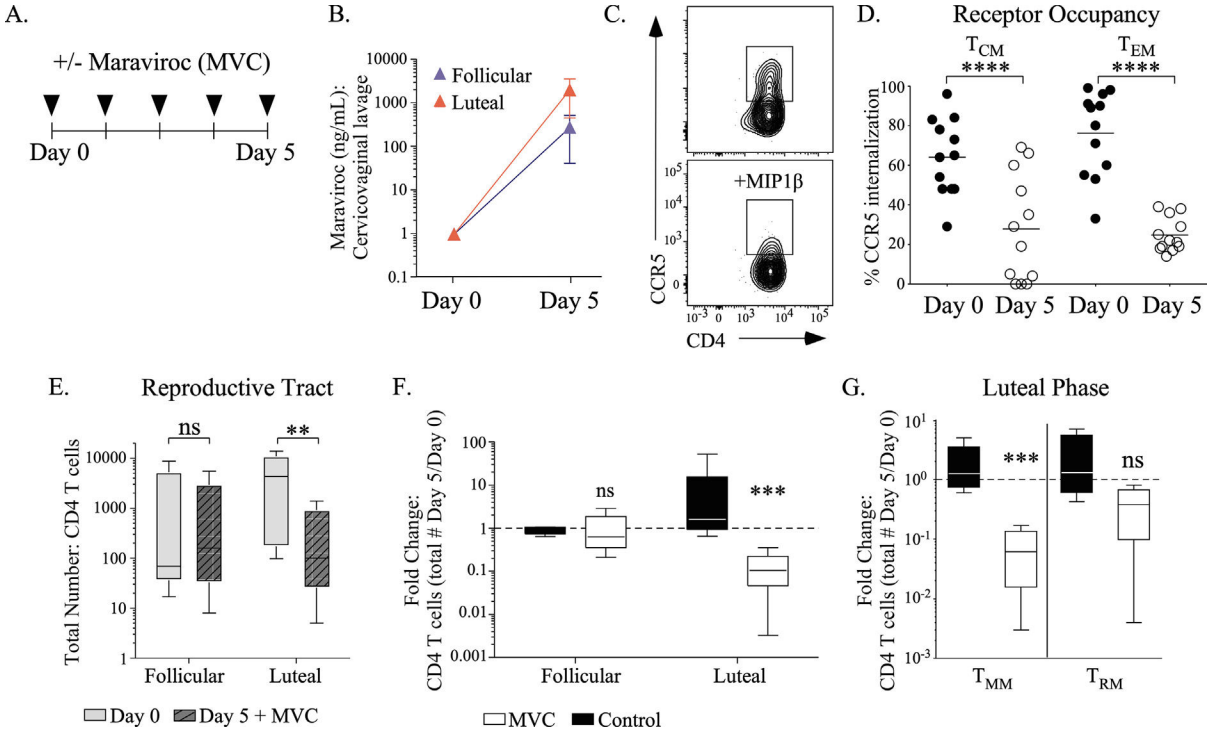

Fig. 5.

Oral Maraviroc inhibits migration of TMM to the FRT during the luteal phase. (A) Schematic diagram of oral Maraviroc (MVC) treatment in six pigtail macaques. Maraviroc was administered daily for 5 days. (B) Maraviroc drug levels in CVL collected at either the follicular or luteal phase of the menstrual cycle prior to (Day 0) or following 5 days of oral Maraviroc treatment (Day 5). (C) Representative flow plots depicting the receptor occupancy assay for measuring CCR5 internalization. CD4 T cells from PBMC were measured for CCR5 following incubation alone (top panel) or following incubation with MIP1β (bottom panel). (D) CCR5 internalization from PBMC CD4 T_{CM} or T_{EM} prior to (black circles) or following 5 days of Maraviroc treatment (white circles). Models evaluating a comparison of means were fit using multiple comparisons. Graph shown as scatter dot plot with mean line. (E) The CVL CD4 T-cell yields (grey box) or following 5 days of Maraviroc treatment (pattern box) during the follicular or luteal phase. (F) The change in CVL CD4 T cells or (G) T_{MM} or T_{RM} (black box) or following 5 days of Maraviroc treatment (white box) during the luteal phase. (E–G) Graphs depicted as box and whiskers plots. Models used to evaluate means were determined by linear regression and fit using generalized estimating equations (GEE). (D–G) The p values with a q value ≤ 0.05 are shown. *$p \leq 0.05$, **$p < 0.01$, ***$p < 0.001$, ****$p < 0.0001$. CD = clusters of differentiation; CVL = cervicovaginal lavage; T_{CM} = central memory CD4 T cells; T_{EM} = effector memory CD4 T cells; T_{MM} = migratory memory T cell; T_{RM} = resident memory T cells.